Final Report

United States Geological Survey Earthquake Hazard Program

Collaborative Project

A systematic approach for discriminating between tectonic and induced earthquake clusters: Collaborative Research with University of Nevada Reno, and University of Southern California

USGA Award Number: G17AP00086

PI: Ilia Zaliapin
University of Nevada Reno
1664 North Virginia st.
Reno, NV, 89557
775-784-6077, 775-784-6378 (fax), zal@unr.edu

USGA Award Number: G17AP00087

PI: Yehuda Ben-Zion
University of Southern California
3651 Trousdale Pkwy, ZHS 117
Los Angeles, CA, 90089-0740
213-740-6106, 213-740-8801 (fax), benzion@usc.edu

Project Start Date: July 31, 2017
Project End Date: July 31, 2018

Abstract

The project focused on developing improved understanding of seismicity and its governing physical processes. The research contributed to developing tools for discriminating between natural and induced earthquakes, gaining insight into the physics of clustered events, and studying the evolution of earthquake clusters in natural and human-induced settings. The project synthesized multiple data sets and state-of-the-art data-analysis techniques. The performed analyses build on recent systematic identification and classification of seismic clusters in relation to properties of the crust and analysis of artifacts produced by common (space-time varying) catalog errors. A key distinguishing aspect of the performed approach is uniform analysis and interpretation of thousands of earthquake clusters on different space-time-energy scales. The methodology can quantify seismicity clustering on time scales of hours to tens of years, and zoom spatially from worldwide analysis to focused studies of selected regions with high-quality data. In addition to advancing the understanding of natural and human-induced seismicity, the obtained results contribute to several backbone topics of statistical seismology. These include (i) definition, detection and classification of seismicity clusters in different environments, (ii) understanding the relative importance of various loading mechanisms, and (iii) understanding deviations from average regional results used typically in analyses of seismicity and hazard. Below we provide additional details on the main results associated with each research direction addressed in this project.

Main Report

1) Comparative Study of Earthquake Clustering in Relation to Hydraulic Activities at Geothermal Fields in California *(Patricia Martínez-Garzón, Ilya Zaliapin, Yehuda Ben-Zion, Grzegorz Kwiatek, and Marco Bohnhoff, 2017)*

This part of the project involved performing a comprehensive analysis of earthquake clustering in three regions characterized by the most active geothermal production in California – The Geysers, Coso, and Salton Sea. We investigate earthquake cluster properties in relation to fluid balance $H(t)$ (the difference of fluid injection and production rates) using nine years of data from The Geysers (both the entire field and a local subset), Coso and Salton Sea geothermal fields in California. Individual earthquake clusters are identified and classified using the nearest-neighbor approach of *Zaliapin and Ben-Zion* (2013a, 2013b); see **Fig. 1.** These are used to calculate nine complementary cluster statistics as time series with a step of about one month; see **Fig. 2**. Three alternative techniques (moving window correlation, analysis of variance, regression) are employed to assess the relations between (possibly non-stationary) time series of cluster statistics and $H(t)$. A total of 108 pairwise relations between cluster statistics and $H(t)$ are analyzed to clarify effects of fluid activities on seismicity in different places. The results of ANOVA analysis are illustrated in **Fig. 3.** The seismic clustering response to the fluid balance differs among the examined fields. The Geysers and Salton Sea areas display the highest and lowest clustering responses, respectively. The proportion of clusters consisting of a single event with no offspring (singles) is correlated significantly with $H(t)$ at all examined datasets, with a lower proportion of singles during periods of high fluid balance. This may reflect increased susceptibility to earthquake triggering in time intervals with high injection rates. The background seismicity rates significantly increase with the fluid balance at the Geysers and Coso, while an opposite relation holds at the Salton Sea. This could be related to the high structural and tectonic complexity at the Salton Sea compared to the other two geothermal fields.

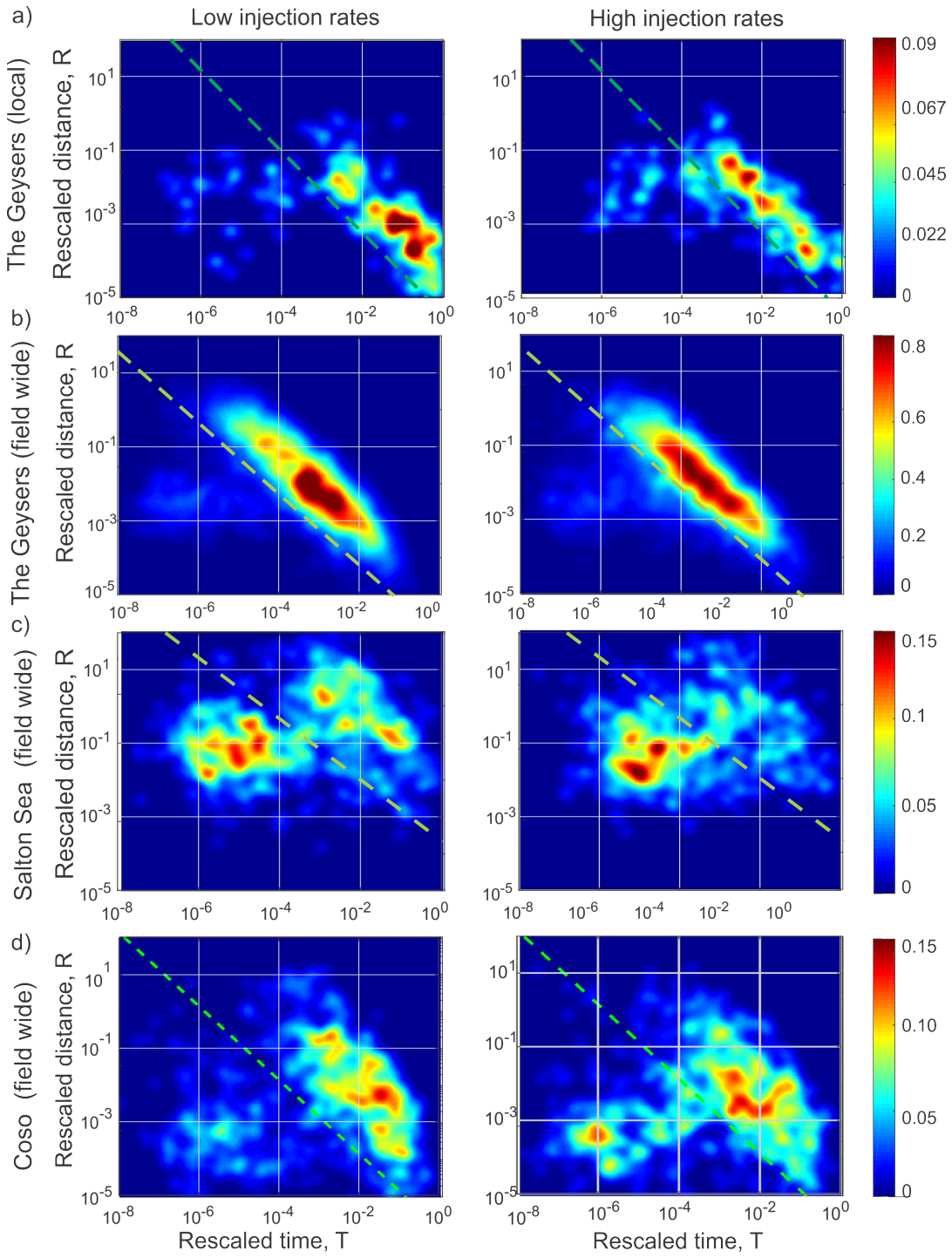

Figure 1: Earthquake proximity. Joint distribution of rescaled time (T) and space (R) components of the earthquake nearest-neighbor proximity $\eta = TR$ for the four analyzed datasets, selecting the 10% of seismicity that occurred closer to local minima and maxima of fluid injection balance (left and right column, respectively). Color bars represent the probability density function. The dashed lines indicate a threshold that separates cluster and background events. (a) The Geysers (local), (b) The Geysers (whole), (c) Salton Sea and (d) Coso.

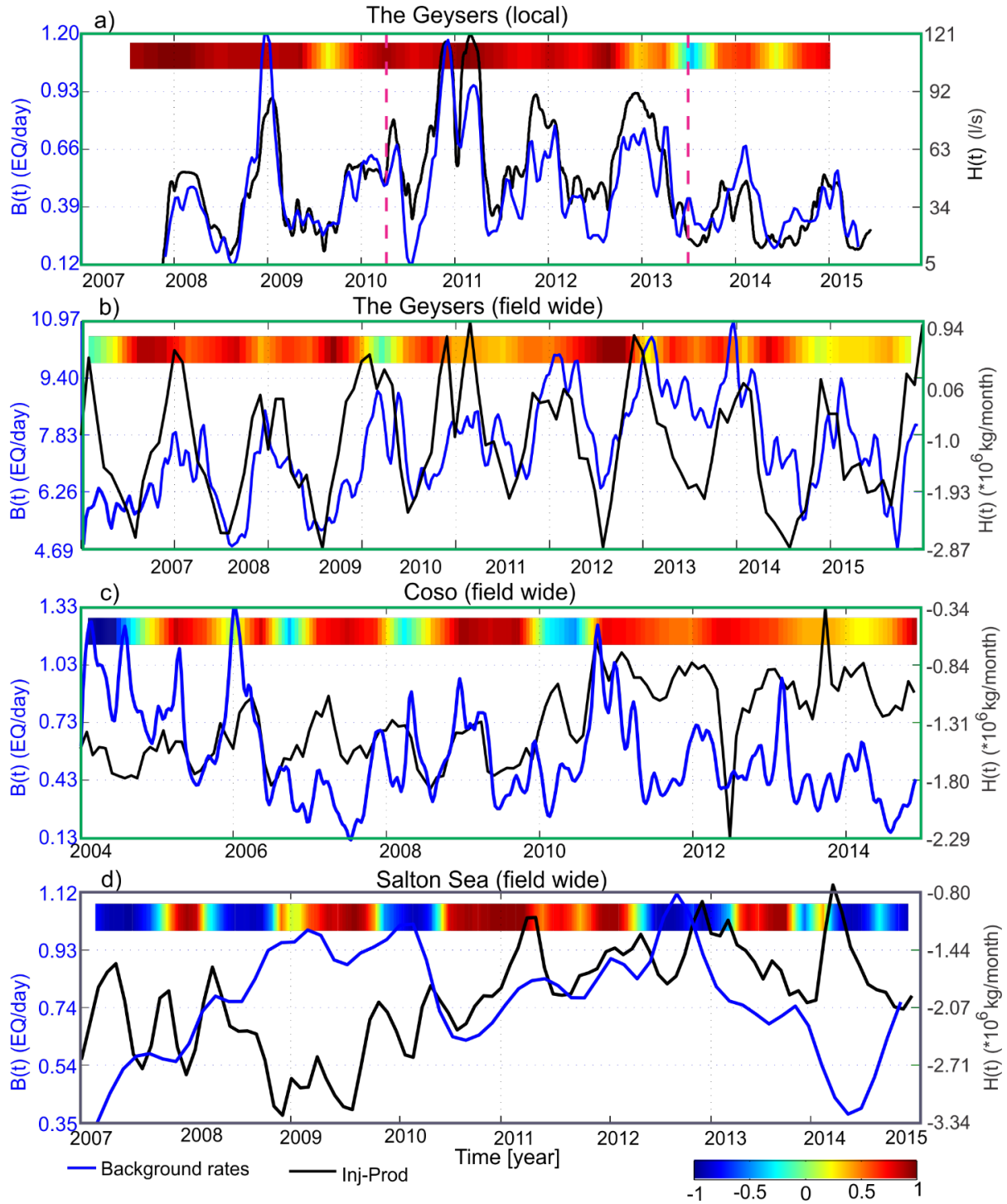

Figure 2: Moving window correlations results. Temporal evolution of the median background seismicity rates ($B(t)$, blue lines) and the fluid balance ($H(t)$, black lines) for (a) The Geysers (local), (b) The Geysers (whole), (c) Coso, and (d) Salton Sea. Note that H(t) at The Geysers (local) represent the injection rates since production is negligible. Dashed magenta lines in (a) mark the start and end of injection in the well Prati-29. Color bars represent the correlation coefficient between the two represented. Each plot is framed in green if the average temporal correlation coefficient is found to be significant ($p < 0.05$).

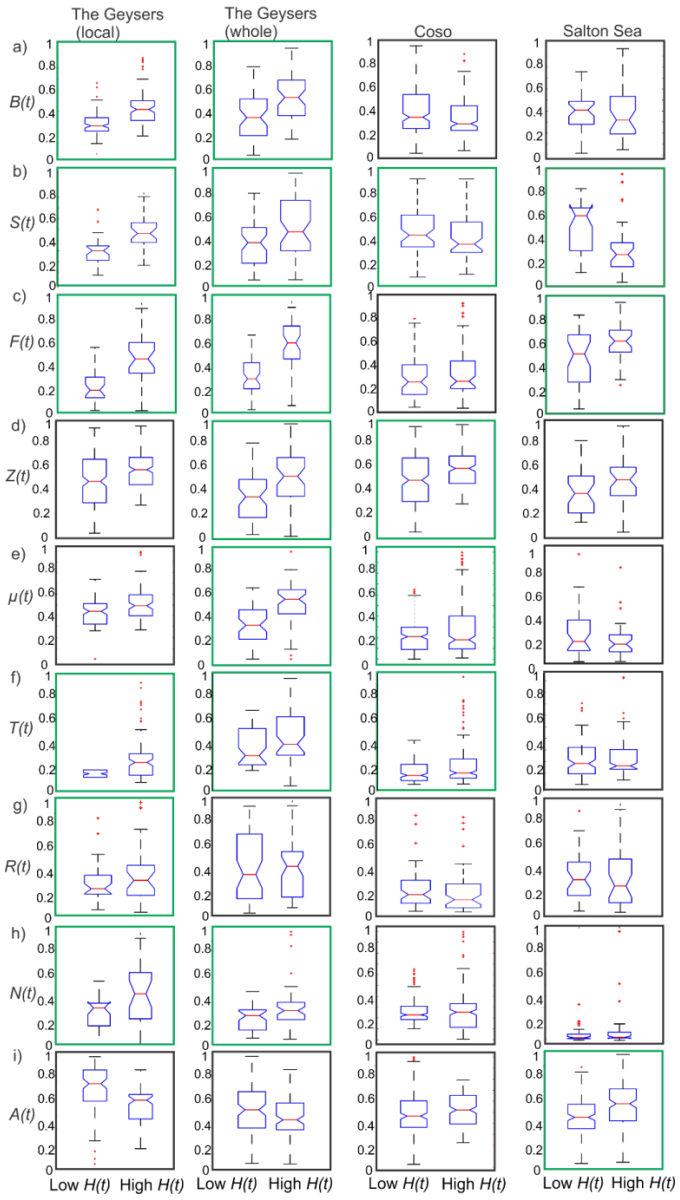

Figure 3: ANOVA analysis results. Multiple statistics that test the null hypothesis H_0: *the means from the populations of* $X(t)$ *during time periods with low and high fluid balance are equal*. The results are illustrated using comparative boxplots for low and high fluid balance periods. In each of the boxplots, the red line indicates the median, the blue box extends between the first and third quartiles, and the black dashed lines (whiskers) extend between the minimum and maximum value excluding outliers, which are shown by red points. Normalized boxplots for The Geysers-local, The Geysers-whole, Coso and Salton Sea are showed in columns from left to right. (a) Background rates $B(t)$, (b) single rates $S(t)$, (c) family rates $F(t)$, (d) proportion of *families* to *singles* $Z(t)$, (e) proximity between events $\mu(t)$, (f) rescaled inter-event time $T(t)$, (g) rescaled inter-event distance $R(t)$, (h) Number of offspring $N(t)$, (i) Proportion of aftershocks to total number of offspring $A(t)$. A box is framed in green if the null hypothesis H_0 is rejected (correlation is found) at 5% significance level.

2) Spatial variations of rock damage production by earthquakes in southern California (*Yehuda Ben-Zion and Ilya Zaliapin, 2018*)

An improved understanding of clustering gained during the project studies allowed us to approach a problem of comparative evaluation of earthquake-related damage production in California during interseismic periods. We performed a comparative spatial analysis of inter-seismic earthquake production of rupture area and volume in southern California using observed seismicity and basic scaling relations from earthquake phenomenology and fracture mechanics. The analysis employs background events from a declustered catalog in the magnitude range $2 < M < 4$ to get temporally stable results representing activity during a typical interseismic period on all faults. The results are illustrated in **Fig. 4**. Regions of relatively high inter-seismic damage production include the San Jacinto fault, South Central Transverse Range especially near major fault junctions (Cajon Pass and San Gorgonio Pass), Eastern CA Shear Zone (ECSZ) and the Brawly seismic zone – Salton Sea area. These regions are correlated with low velocity zones in detailed tomographic studies. A quasi-linear zone with ongoing damage production extends between the Imperial fault and ECSZ and may indicate a possible future location of the main plate boundary in the area. The regions around the 1992 M6.1 Joshua Tree, M7.3 Landers and M6.3 Big Bear earthquakes have background seismic activity before 1990. This may represent a regional weakening process by damage production in future rupture zones. The depth of background seismicity and damage production decreases steadily from SW of the coastline to NE of the San Andreas fault, and also to the SE near the US-Mexico border. The seismicity and rock damage become more pronounced and continuous along-strike of main faults with increasing depth. The methodology and results on estimated seismic production of rock damage are useful for separating effects associated with rock composition and damage in tomographic images, and can help quantifying generation of rock damage in induced seismicity.

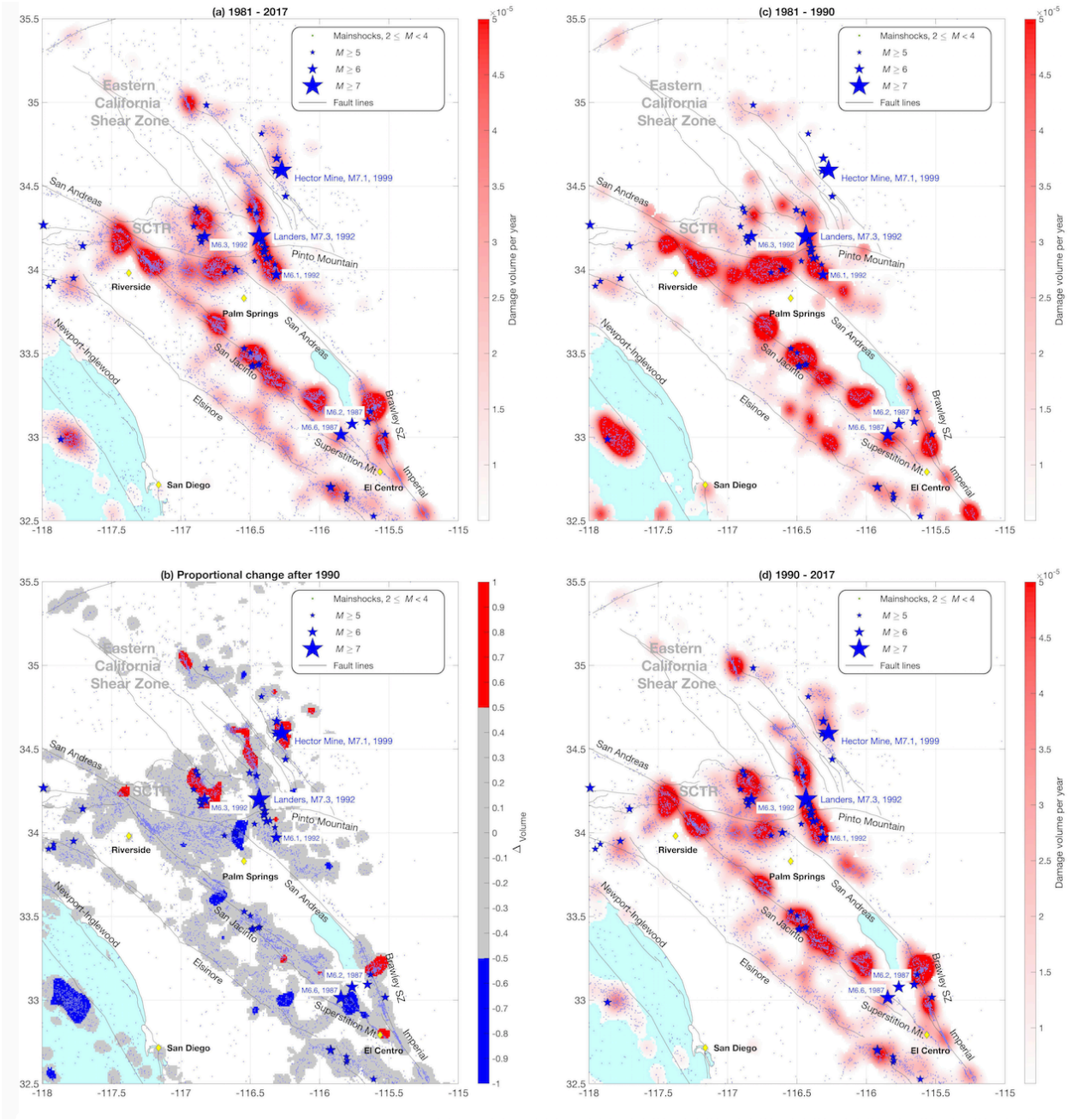

Figure 4. Interseismic damage. Estimation of interseismic damage volume V in km^3 yr^{-1} – a surface projection. The damage is estimated using background events with magnitude $2 \le M < 4$; they are shown by dots. (a) The damage volume (color code) estimated during 1981 – 2017. (b) Proportional change Δ_{volume} in the damage volume production after 1990, as defined by Eq. (13). The values $\Delta_{volume} > 0.5$ (damage increase) are shown in red, $\Delta_{volume} < -0.5$ (damage decrease) are shown in blue, and all other values are gray. (c) The damage volume (color code) estimated during 1981 – 1990. (d) The damage volume (color code) estimated during 1990 – 2017. The damage values in panels (a), (c), and (d) are clipped at 5×10^{-5}; the values below 5×10^{-6} are transparent.

3) Systematic detection and classification of earthquake clusters in Italy (*Piero Poli, Yehuda Ben-Zion, and Ilya Zaliapin, 2018*)

This part of the project extends earthquake cluster analysis to other seismogenic regions, to test the validity of our findings in California and exploring other cluster regimes. We perform a systematic analysis of spatio-temporal clustering of 2007-2017 earthquakes in Italy with magnitudes $m > 3$. The study employs the nearest-neighbor approach of *Zaliapin and Ben-Zion* (2013a, 2013b) with basic data-driven parameters. The results indicate that seismicity in Italy, which is dominated by an extensional tectonic regime, is dominated by clustered events, with smaller proportion of background events than in California. Evaluation of internal cluster properties allows separation of swarm-like from burst-like clusters. This classification highlights a strong geographical coherence of cluster properties. Swarm-like seismicity are dominant in regions characterized by relatively slow deformation with possible elevated temperature and/or fluids (e.g. Alto Tiberina, Pollino), while burst-like seismicity is observed in crystalline tectonic regions (Alps and Calabrian Arc) and in Central Italy where moderate to large earthquakes are frequent (e.g. L'Aquila, Amatrice). To better assess the variation of seismicity style across Italy, we also perform a clustering analysis with region-specific parameters (**Fig. 5**). This analysis highlights clear spatial changes of the threshold separating background and clustered seismicity and permits better resolution of different clusters in specific geological regions. For example, a large proportion of repeaters is found in the Etna region as expected for volcanic-induced seismicity. A similar behavior is observed in the northern Apennines with high pore pressure associated with mantle degassing. The observed variations of earthquakes properties highlight shortcomings of practices using large-scale average seismic properties, and points to connections between seismicity and local properties of the lithosphere. The observations help to improve the understanding of the physics governing the occurrence of earthquakes in different regions.

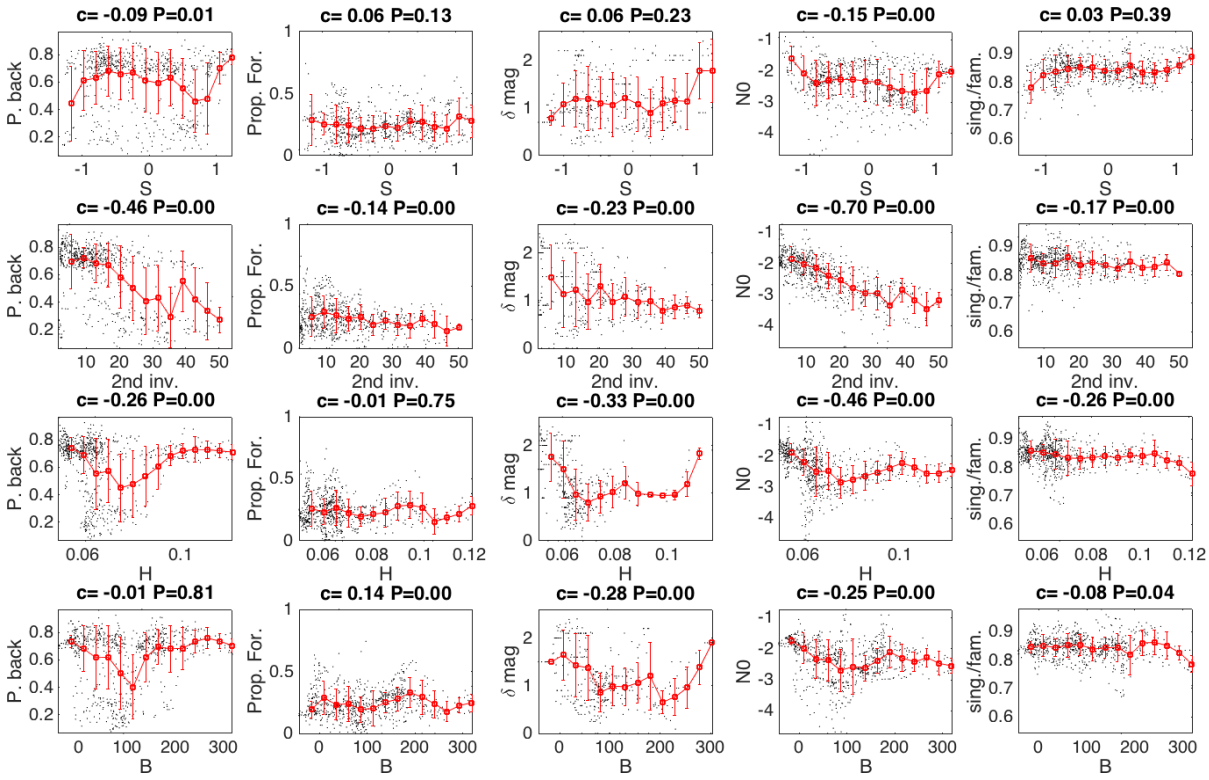

Figure 5: Scatter plot comparing deformation style S, 2nd invariant I of the stress rate tensor, heat flow H, and Bouguer anomaly G against proportion B of background events, proportion F of foreshocks, proximity threshold η_0, and proportion of singles. Black dots correspond to individual clusters, while the red error bar plot is obtained by estimating the average and standard deviation over 15 evenly spaced intervals along the x-axis. The Spearman's correlation coefficient c and respective P-value are reported in top of each plot.

Project Data: The project did not generate new data. The data processing algorithms developed during the project, the results of respective catalog analysis and interpretation of findings are all published in peer-review journals (see references below).

Acknowledgment of Support: This material is based upon work supported by the U.S. Geological Survey under Grant Nos. G17AP00086, G17AP00087.

Disclaimer: The views and conclusions contained in this document are those of the authors and should not be interpreted as representing the opinions or policies of the U.S. Geological Survey. Mention of trade names or commercial products does not constitute their endorsement by the U.S. Geological Survey.

Project Publications

1. Martínez-Garzón, P., I. Zaliapin, Y. Ben-Zion, G. Kwiatek and M. Bohnhoff (2017) Comparative study of earthquake clustering in relation to hydraulic activities at geothermal fields in California, *J. Geophys. Res.*, https://doi.org/10.1029/2017JB014972
2. Ben-Zion, Y. and I. Zaliapin (2018) Spatial variations of rock damage production by earthquakes in southern California. *In review.*
3. Poli, P., Y. Ben-Zion, and I. Zaliapin (2018) Systematic detection and classification of earthquake clusters in Italy. *ms in preparation*.

References used in the report

1. Zaliapin, I. and Y. Ben-Zion (2013a) Earthquake clusters in southern California, I: Identification and stability. *J. Geophys. Res*., 118, 2847-2864. doi: 10.1002/jgrb.50179
2. Zaliapin, I. and Y. Ben-Zion (2013b) Earthquake clusters in southern California, II: Classification and relation to physical properties of lithosphere. *J. Geophys. Res*., 118, 2865-2877. doi: 10.1002/jgrb.50178